Study of $(\alpha, \alpha n)$ Reactions with 900-MeV Helium Ions

L. B. Church

Department of Chemistry, State University of New York, Buffalo, New York 14214

(Received 8 May 1972; revised manuscript received 2 August 1972)

Cross sections for $(\alpha, \alpha n)$ reactions on ^{58}Ni, ^{65}Cu, and ^{197}Au at 900 MeV have been determined relative to the ^{27}Al$(\alpha, \alpha 2pn)^{24}$Na monitor reaction. They are 49.3 ± 3.5, 64.6 ± 2.8, and 95.8 ± 1.4 mb, respectively. The cross section used for the monitor reaction at this energy was 22.0 mb; this was determined through a comparison of the ^{24}Na and ^{18}F activities produced in Al foil by 920-MeV helium ions. The general trends observed in $(\alpha, \alpha n)$ cross sections as a function of target composition are discussed. The direct population of the (12−) to (2−) states of ^{196}Au is 0.07 and this suggests a mechanism of direct emission of the neutron from the target surface. The observed trend of $\sigma(\alpha, \alpha n)$ with the neutron skin thickness of the target also supports this mechanism. These reactions are compared with the high-energy (p, pn) reactions of the same targets.

I. INTRODUCTION

The $(\alpha, \alpha n)$ nuclear reaction[1] induced by high-energy helium ions incident upon complex nuclei can occur by several different reaction mechanisms. For example, the incident ion can cause the direct emission of a neutron and leave the residual nucleus with insufficient energy to cause the evaporation of any other nucleons. This sequence of events implies that the reaction finishes before the residual nucleus can attain equilibrium and that the helium ion retains its identity during the course of the nuclear reaction. An alternative mechanism is a two-step sequence of events in which the helium ion causes the emission of several nucleons. The reaction finishes with the evaporation of the remaining necessary particles from an excited nuclide in equilibrium. In the later mechanism, it is possible for the projectile to be partly or totally incorporated into the target nucleus and thus lose its identity.

To date, little work has gone into the study of simple high-energy helium-ion-induced reactions. This is in part because there are few (perhaps two) machines capable of accelerating these ions to the 900-MeV region. For example, the only high-energy ($\gtrsim$700 MeV) $(\alpha, \alpha n)$ cross sections measured to date have been on ^{12}C and ^{16}O by Radin and co-workers,[2,3] and on ^{127}I by Ladenbauer and Winsberg.[4] However, neither of these investigations concentrated on a determination of the importance of each reaction mechanism.

Another investigation relevant to the present study was by Igo, Hansen, and Gooding[5] on the $(\alpha, 2\alpha)$ reaction. Their results indicate a strong probability for α clusters near the nuclear surface and for quasielastic collisions between the incoming helium ion and these clusters. Extrapolation of these conclusions to the present $(\alpha, \alpha n)$ study would suggest that the simple one-step or clean-knockout (CKO) mechanism should occur more often than the mechanism of total or partial helium-ion incorporation with subsequent nucleon evaporation. Likewise recent studies of high-energy (p, pn) reactions[6-12] have shown that the CKO mechanism predominates with most targets; however, its importance diminishes with the heavier masses. In the present study the specific targets were selected because of the previous (p, pn) work accomplished with them.

The objectives of the present work were to measure the $(\alpha, \alpha n)$ cross sections for a number of interesting targets, to ascertain the general trends that these reactions display as a function of target composition, and to then use these data to try to determine the primary $(\alpha, \alpha n)$ reaction mechanism for each target.

II. EXPERIMENTAL PROCEDURES

A. Targets and Irradiations

The cross sections were determined by conventional techniques using the internal helium-ion beam of the Lawrence Berkeley Laboratory 184-in. synchrocyclotron. The targets were bombarded at a radial position and in a magnetic field corresponding to a beam energy of 900 MeV.

The nickel targets were fabricated by electroplating isotopically enriched (99.9%) ^{58}Ni to a surface density of about 5 mg cm^{-2} onto 0.08-mm-thick gold foil. The copper targets were enriched (99.7%) ^{65}Cu electroplated onto 0.08-mm-thick titanium foil to a thickness of about 8 mg cm^{-2}. The gold targets were 0.08-mm-thick, 99.9% pure foils. During the irradiation all targets were flanked by a set of 99.9% pure aluminum foils: two 0.04-mm-thick inner guard foils, two 0.08-mm-thick beam-monitor foils, and two 0.04-mm-

thick outer guard foils. The outer guard foils protected the target assembly and compensated for recoils out of the monitor foils; they were discarded after the irradiation. The inner guard foils also compensated for recoils out of the monitor foils and caught recoils originating in the target; they were dissolved along with the target.

After bombardment the targets were taken to the chemistry laboratory where a 1.0-cm-diam disk was punched out close to the front or leading edge. The alignment of the different foils during the irradiation and punching was checked by comparing the difference in activity between the two monitor foils; this difference was usually less than 1% of their average. The ^{65}Cu and ^{58}Ni targets were dissolved in the presence of a known amount of additional carrier to bring the elemental concentration up to about 15 mg. The desired products were separated and purified from about 10 mg each of the appropriate holdback carriers using standard radiochemical techniques.[13] Final precipitates were filtered onto glass filter paper, dried and mounted for counting. The chemical yield for each sample was determined after counting using atomic absorption spectroscopy.

In order to determine the contribution from the aluminum guard foils and the gold or titanium backing foils to the products of the ^{58}Ni and ^{65}Cu targets, a blank target was irradiated with the normal beam intensity. The activity of the products in the blank run was less than 1% when compared to one of the normal irradiations and was therefore ignored.

B. Helium-Ion-Beam Monitor

The helium-ion beam was monitored using the ^{27}Al(α, $\alpha 2pn$)^{24}Na reaction. The cross section of this reaction was determined relative to the ^{27}Al-(α, $3\alpha n$)^{18}F cross section which has been reported by Radin *et al.*[3] for 920-MeV helium ions. In the separate series of experiments to determine the monitor cross section, a 0.08-mm-thick 99.99% pure Al target foil and guard foils were irradiated in the 920-MeV external helium-ion beam. The ^{18}F and ^{24}Na β activities in the Al foil were counted without chemical separation as described in Sec. II C.

The ^{27}Al(α, $\alpha 2pn$)^{24}Na monitor cross section as determined in two individual irradiations was 22.0 ± 2.0 mb. The 9% total uncertainty is the standard deviation of both the random and systematic sources of error in the measurements. The random uncertainty between the two determinations was ±1% and the systematic uncertainties include the β-counting efficiencies (±8%), and the ^{27}Al(α, $3\alpha n$)-^{18}F cross section (±4%) reported in Ref. 3.

C. Counting

The decay rates for the ^{57}Ni, ^{196m}Au, and ^{196g}Au were determined using a 7-cm^3 Ge(Li) detector in connection with a multichannel analyzer. The efficiency of the detector was determined as a function of γ-ray energy using several different sets of International Atomic Energy Agency standards. The decay rates of the ^{64}Cu were determined by counting the β radiations with an end-window proportional counter. The counting efficiency of this β counter was determined for each of these nuclides by counting several other similarly prepared sources whose absolute disintegration rate had been determined by counting the γ radiations of each nuclide with the aforementioned Ge(Li) detector. The radiations measured for each product nuclide, along with the important decay scheme data are summarized in Table I.

TABLE I. Decay schematics. All data were taken from C. M. Lederer, J. M. Hollander, and I. Perlman, *Table of Isotopes* (Wiley, New York, 1967).

Nuclide	Half-life	Mode of decay	Maximum energy (MeV)	Branching abundance
^{18}F	110 min	β^+	0.64	0.97
		γ	0.511	1.94
^{24}Na	15.0 h	β^-	1.39	1.00
		γ	1.37	1.00
^{57}Ni	36.0 h	γ	1.37	0.86
^{64}Cu	12.8 h	β^-	0.57	0.38
		β^+	0.66	0.19
		γ	0.511	0.38
^{196m}Au	9.7 h	γ	0.148	0.42
^{196g}Au	6.18 day	γ	0.33 + 0.356	1.19

III. RESULTS

Cross sections were calculated by the standard method which included a least-squares extrapolation of the product activities to the end of bombardment.[14] The average cross section for three individual determinations of each target is listed in Table II along with the random standard deviation, which averages about 5%.

TABLE II. Product cross sections using 900-MeV helium ions and ^{27}Al(α, $\alpha 2pn$)^{24}Na as the monitor reaction with a cross section of 22.0 mb.

^{58}Ni(α, αn)^{57}Ni	49.3 ± 3.5 mb
^{65}Cu(α, αn)^{64}Cu	64.6 ± 2.8 mb
^{197}Au(α, αn)^{196m}Au	6.0 ± 0.6 mb
^{197}Au(α, αn)^{196}Au (total)	95.8 ± 1.4 mb

In addition to the uncertainties listed in Table II, each cross section has additional systematic uncertainties, such as the monitor cross section, which should be taken into account in evaluating the total uncertainty associated with the cross section. When the systematic uncertainties are estimated, a total standard deviation is calculated to be less than 20% for all the cross sections listed in Table II.

IV. DISCUSSION

A. Trends of the $(\alpha, \alpha n)$ Cross Sections

In order to study the general trends of high-energy $(\alpha, \alpha n)$ cross sections as a function of target composition, the three cross sections listed in Table II are complemented with the three $(\alpha, \alpha n)$ cross sections of Refs. 2–4. The ^{127}I cross section reported by Ladenbauer and Winsberg[4] at 720 MeV is first adjusted to a 23-mb ^{27}Al$(\alpha, \alpha 2pn)^{24}$Na monitor cross section at that energy and then extrapolated to 900 MeV. This procedure yields a value of 70 ± 10 mb for the ^{127}I$(\alpha, \alpha n)^{126}$I cross section. The cross sections of Radin *et al.* on ^{12}C and ^{16}O are used as reported.[2,3]

These six cross sections are shown in Fig. 1 as a function of the target mass, and in Fig. 2 as a function of the target's N/Z ratio. A comparison of these two figures shows that the $\sigma(\alpha, \alpha n)$ increases with both A and N/Z; however, the trend of Fig. 2 is much more linear than Fig. 1. A small deviation from the general trend is noted in the low-A region (^{12}C and ^{16}O) of Fig. 1; this may, in part, be the result of the often-studied α-particle clustering present in these light nuclei. It would be interesting to continue to study the trend observed in Fig. 2 by measuring $\sigma(\alpha, \alpha n)$ for other targets far removed from β stability.

There are now sufficient data available to be able to start to compare the trends of $\sigma(\alpha, \alpha n)$ with $\sigma(p, pn)$; for example, compare Fig. 1 of Ref. 7 with Fig. 1 of this report. The (p, pn) data contain three main characteristics as A increases: (i) There is a large variation in $\sigma(p, pn)$ from target to target when $A \lesssim 20$; (ii) the onset of a wide range of targets ($A \gtrsim 20$) whose $\sigma(p, pn)$ is close to 60 mb with (iii) the exception of a small number of targets (such as ^{58}Ni) with cross sections near 30 mb. Two of these three characteristics can be seen in Fig. 1. The already mentioned deviation away from the general trend for the ^{12}C and ^{16}O targets can be compared to the light mass (p, pn) targets. Similar to the $\sigma(p, pn)$ trend, there is a sharp increase in the $(\alpha, \alpha n)$ cross sections between the ^{58}Ni and ^{65}Cu targets despite the proximity of their masses. The abundance of $\sigma(p, pn)$ data shows that the ^{58}Ni is low when compared to other nearby targets such as ^{50}Cr, ^{64}Zn, and ^{65}Cu. With the present $\sigma(\alpha, \alpha n)$ data available, it is not possible to determine for sure if the ^{58}Ni cross section is also unusually low, but the trend as seen in Fig. 1 would suggest that this is, indeed, the case.

A significant deviation between the (p, pn) and $(\alpha, \alpha n)$ studies occurs when the trend in the medium to heavier ($A \gtrsim 60$) target region is compared. The $\sigma(p, pn)$ cross section does not increase significantly (about 10%) between ^{65}Cu and ^{197}Au. Yet, as can be seen in Fig. 1, the $\sigma(\alpha, \alpha n)$ increases by about 40% over this same mass region.

The ratios of $\sigma(\alpha, \alpha n)$ (Table II) to the corresponding $\sigma(p, pn)$ (interpolated from Caretto[15] to 900 MeV) vary between 1.8 and 1.4 with an average at 1.6. This is generally consistent with the

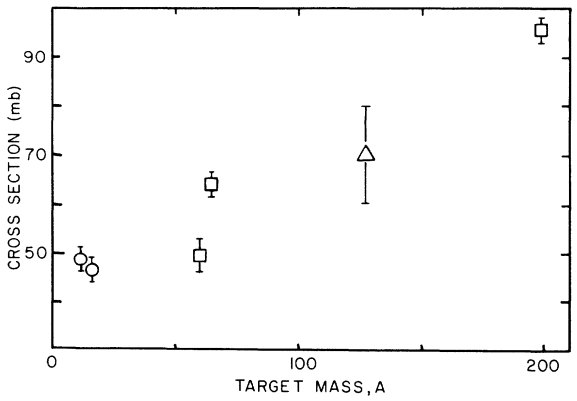

FIG. 1. Cross sections for $(\alpha, \alpha n)$ reactions at 900 MeV as a function of target mass. Circles are from Refs. 2 and 3, triangle is extrapolated from Ref. 4, and squares are from the present work.

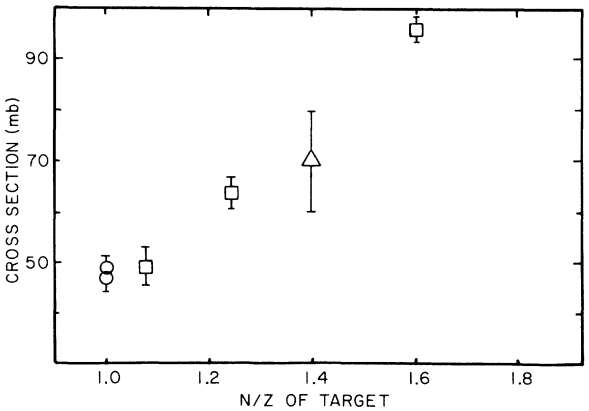

FIG. 2. Cross sections for $(\alpha, \alpha n)$ reactions at 900 MeV as a function of target's N/Z ratio. Circles are from Refs. 2 and 3, triangle is extrapolated from Ref. 4, and squares are from the present work.

ratios on ^{12}C and ^{16}O as reported by Radin *et al.*,[2,3] and with the more complex reactions on ^{93}Nb as reported by Korteling and Hyde.[16]

B. $(\alpha, \alpha n)$ Reaction Mechanism

While the general trends of the $\sigma(\alpha, \alpha n)$ values discussed in Sec. IV A are interesting, especially when compared to the (p, pn) cross sections, they offer little real help in the analysis of the reaction mechanism. However, the ratio of the production cross sections for the two ^{196}Au isomeric levels can assist in an analysis of the angular momentum transferred to the target nuclide during the $(\alpha, \alpha n)$ reaction, and this can be used to understand the reaction mechanism. For example, by assuming a clean knockout of one of the outer neutrons of the ^{197}Au target (spin $\frac{3}{2}+$) by the incident helium ion, the ratio of direct population of the (12−) ^{196m}Au to the (2−) ^{196g}Au states can be calculated. This same approach was recently taken in a study[17] of the 400-MeV (p, pn) reaction on ^{197}Au.

The well-known method of Vandenbosch and Huizenga[18] was used in this calculation along with the shell-model calculation of the neutron levels of the ^{197}Au nucleus by Ross, Mark, and Lawson.[19] The results of this calculation are shown in Fig. 3 and only the top four levels were considered because deeper neutron levels would have involved excitation energies large enough to permit further particle evaporation. The relative probability of the clean knockout of a neutron from these levels was calculated from the product of the number of neutrons in the level n and Benioff's fractional availability coefficients, M_{nl}.[20] Because of the ratio nature of these calculations, any error introduced by using these M_{nl} values (which were calculated from the data of GeV energy proton bombardments) in an application with 900-MeV helium ions is probably small. The removal of a neutron with angular momentum J_n results in a set of states having angular momentum $J_f = |J_n + \frac{3}{2}|$ to $J_f = |J_n - \frac{3}{2}|$ and with relative weights, R_j, varying for each neutron level as $(2J_f + 1)$. The deexcitation of nuclei with this set of spins was assumed to occur with quadrupole γ rays averaging 2 MeV each. The calculation was performed using a spin parameter σ of 4.0 and assuming that the last γ ray resulted in the popula-

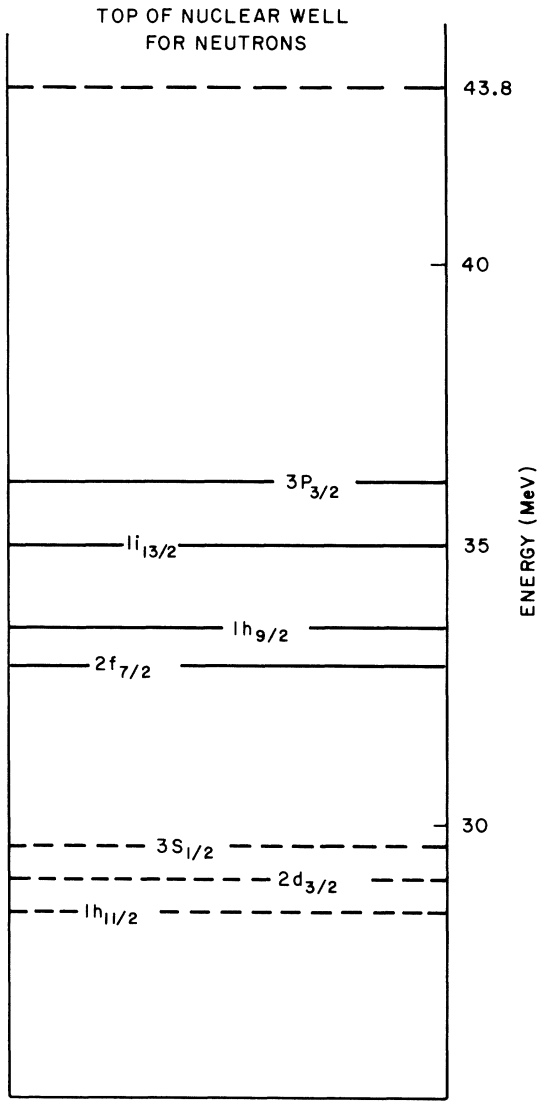

FIG. 3. The top neutron levels of ^{197}Au as calculated in Ref. 19.

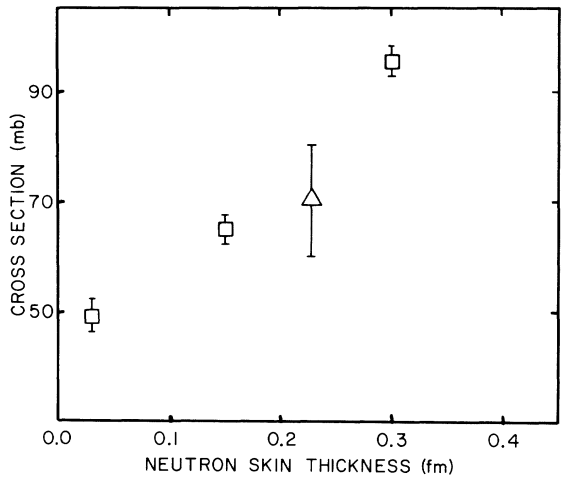

FIG. 4. Cross sections for the heavier mass $(\alpha, \alpha n)$ reactions at 900 MeV as a function of target's neutron skin thickness (see text and Ref. 21). Triangle is extrapolated from Ref. 4 and squares are from the present work.

tion of either the (12−) or (2−) isomer of ^{196}Au, depending on which transition involved a smaller spin change.

The calculated ratio of the population of the (12−) to (2−) isomeric states is 0.15; this can be compared to the experimental ratio taken from Table II of 0.07. The low experimental ratio and a favorable comparison to the calculated ratio supports the direct or one-step neutron-emission mechanism. For if part or all of the helium ion were incorporated into the ^{197}Au target nucleus, then the resulting angular momentum should have been reflected in a larger (12−)/(2−) isomeric ratio. A comparison of the experimental $(\alpha, \alpha n)$ isomeric ratio (0.07) and that part of the experimental (p, pn) isomeric ratio (0.18) due to the CKO mechanism[17] suggests that perhaps the site of the helium-ion-neutron interaction is localized more to the outermost $3P_{3/2}$ neutrons than is the proton-neutron interaction in the (p, pn) reaction.

If, as the ^{196}Au isomeric ratio suggests, the $(\alpha, \alpha n)$ reaction mechanism is the clean knockout of an outer neutron, then the cross section should, in part, be determined by the abundance of neutrons on the outer edge of the target. To a certain extent, this is confirmed by Fig. 2 where $\sigma(\alpha, \alpha n)$ increases with increasing N/Z. An alternative way of examining this idea is to compare the neutron skin thickness as a function of $\sigma(\alpha, \alpha n)$. The neutron skin thickness for each target can be calculated using the equation of Myers[21] and this value is plotted against $\sigma(\alpha, \alpha n)$ in Fig. 4. The linear variation exhibited in Fig. 4 lends credence to, but does not prove, the hypothesis of a CKO $(\alpha, \alpha n)$ reaction mechanism.

V. CONCLUSIONS

It might be argued that it is unwise to generalize on an entire set of reactions using only six measured $(\alpha, \alpha n)$ cross sections; especially when, after two decades of work, there are many facets of the similar (p, pn) reaction which are not fully understood. Nevertheless, the $\sigma(\alpha, \alpha n)$ measured to date increase rather regularly with increasing N/Z and less regularly with target mass. When compared to high-energy (p, pn) results, the $\sigma(\alpha, \alpha n)$ differ most significantly in the trends observed in the medium-to-heavy mass region $(A \gtrsim 60)$. An analysis of the ^{197}Au$(\alpha, \alpha n)^{196}$Au isomeric ratio and the variation of $\sigma(\alpha, \alpha n)$ with neutron skin thickness suggests a one-step $(\alpha, \alpha n)$ reaction mechanism. The direct emission of a neutron would most likely occur on the peripheral regions of the nucleus, and thus the projectile probably retains its identity throughout the reaction.

ACKNOWLEDGMENTS

The author wishes to thank Dr. Earl K. Hyde for helping to provide a summer fellowship at Lawrence-Berkeley Laboratory (LBL) which made this work possible. He is also grateful to Dr. J. Howard and the rest of the Medical Physics group at LBL for their assistance with the external beam, to J. Vale for arranging the internal beam irradiations, and to N. Jacobs for his valuable assistance in the laboratory. This work was, in part, sponsored by a grant from the Research Corporation; this financial assistance is gratefully acknowledged.

---

[1]In the context of this paper, the use of $(\alpha, \alpha n)$ is not meant to imply a particular reaction mechanism, but simply shows the relationship between the target and product of interest.

[2]J. Radin, Phys. Rev. C 2, 793 (1970); 4, 1010 (1971).

[3]J. R. Radin, S. A. Karff, A. R. Smith, and N. Little, U. S. Atomic Energy Commission Report No. UCRL-20 121, 1971 (unpublished).

[4]I.-M. Ladenbauer and L. Winsberg, Phys. Rev. 119, 1368 (1960).

[5]G. Igo, L. F. Hansen, and R. J. Gooding, Phys. Rev. 131, 337 (1963).

[6]J. R. Grover and A. A. Caretto, Jr., Ann. Rev. Nucl. Sci. 14, 51 (1964).

[7]P. J. Karol and J. M. Miller, Phys. Rev. 166, 1089 (1968).

[8]L. P. Remsberg, Phys. Rev. 174, 1338 (1968).

[9]Y.-W. Yu, A. A. Caretto, Jr., and L. B. Church, Nucl. Phys. A152, 295 (1970).

[10]J. A. Panontin, L. L. Schwartz, A. F. Stehney, and E. P. Steinberg, Phys. Rev. 145, 754 (1966); 169, 851 (1968).

[11]W. J. Nieckarz, Jr., and A. A. Caretto, Jr., Phys. Rev. C 2, 1917 (1970).

[12]R. F. Schall, Jr., and A. A. Caretto, Jr., Phys. Rev. C 2, 1924 (1970).

[13]National Academy of Sciences – National Research Council Nuclear Science Series, Reports Nos. NAS-NS-3027, -3051, and -3036 (unpublished).

[14]J. B. Cumming, National Academy of Sciences – National Research Council Report No. NAS-NS-3107, 1961 (unpublished), p. 25.

[15]A. A. Caretto, Jr., U. S. Atomic Energy Commission Report No. NYO-10693, 1964 (unpublished).

[16]R. G. Korteling and E. K. Hyde, Phys. Rev. 136, B425 (1964).

[17]L. B. Church, J. Inorg. Nucl. Chem. 33, 909 (1971).

[18]R. Vandenbosch and J. R. Huizenga, Phys. Rev. 120, 1313 (1960); 120, 1305 (1960).

[19]A. A. Ross, H. Mark, and R. D. Lawson, Phys. Rev. 102, 1616 (1956).

[20]P. A. Benioff, Phys. Rev. 119, 324 (1960).

[21]W. D. Myers, Phys. Letters 30B, 451 (1969).